



Published in final edited form as:

*Sci Signal*. ; 11(524): . doi:10.1126/scisignal.aao4180.

## The nociceptin receptor inhibits axonal regeneration and recovery from spinal cord injury

Yuichi Sekine, Chad S. Siegel, Tomoko Sekine-Konno, William B. J. Cafferty, and Stephen M. Strittmatter\*

Cellular Neuroscience, Neurodegeneration and Repair Program, Interdepartmental Neuroscience Program, Departments of Neurology and Neuroscience, Yale University School of Medicine, New Haven, CT 06536, USA.

### Abstract

Axonal growth after traumatic spinal cord injury is limited by endogenous inhibitors, selective blockade of which promotes partial neurological recovery. The partial repair phenotypes suggest that compensatory pathways limit improvement. Gene expression profiles of mice deficient in *Ngr1*, which encodes a receptor for myelin-associated inhibitors of axonal regeneration such as Nogo, revealed that trauma increased the mRNA expression of *ORL1*, which encodes the receptor for the opioid-related peptide nociceptin. Endogenous and overexpressed ORL1 coimmunoprecipitated with immature NgR1 protein, and ORL1 enhanced the O-linked glycosylation and surface expression of NgR1 in HEK293T and Neuro2A cells and primary neurons. ORL1 overexpression inhibited cortical neuron axon regeneration independently of NgR1. Furthermore, regeneration was inhibited by an ORL1 agonist and enhanced by the ORL1 antagonist J113397 through a ROCK-dependent mechanism. Mice treated with J113397 after dorsal hemisection of the mid-thoracic spinal cord recovered greater locomotor function and exhibited lumbar raphespinal axon sprouting. These effects were further enhanced by combined *Ngr1* deletion and ORL1 inhibition. Thus, ORL1 limits neural repair directly and indirectly by enhancing NgR1 maturation, and ORL1 antagonists enhance recovery from traumatic CNS injuries in wild-type and *Ngr1* null mice.

---

exclusive licensee American Association for the Advancement of Science. No claim to original U.S. Government Works

\*Corresponding author. stephen.strittmatter@yale.edu.

Author contributions:

Y.S. conducted the majority of the experiments. C.S.S. contributed to the SCI experiments and T.S.-K. to the cell culture experiments. Y.S., W.B.J.C., and S.M.S. conceived the study, analyzed the data, and wrote the manuscript.

SUPPLEMENTARY MATERIALS

[www.sciencesignaling.org/cgi/content/full/11/524/eaao4180/DC1](http://www.sciencesignaling.org/cgi/content/full/11/524/eaao4180/DC1)

Competing interests:

S.M.S. is a cofounder of ReNetX Bio, which seeks to develop NgR1-based therapeutics. All the other authors declare that they have no competing interests.

Data and materials availability:

The RNA microarray data are available from Mendeley (<https://data.mendeley.com>, doi:10.17632/d5cz46zv8z.1). All other data required to evaluate the conclusions in the paper are present in the paper or the Supplementary Materials.

## INTRODUCTION

After traumatic spinal cord injury (SCI), and multiple other forms of neurological injury, the interruption of axonal tracts leads to disconnection of neurons and loss of function. There is little regrowth of fibers in the adult mammalian brain or spinal cord; fiber growth is limited by both cell-intrinsic factors, such as phosphatase and tensin homolog (PTEN) (1, 2), Krüppel-like factors (KLFs) (3), or suppressor of cytokine signaling 3 (SOCS3) (4), and cell-extrinsic factors, such as chondroitin sulfate proteoglycan (CSPG) (5, 6) or myelin-associated inhibitors (7–15). Expression of other genes, such as *dlk-1* (16, 17) (which encodes dual leucine zipper kinase and is homologous to *MAP3K12*), is required both for neurodegenerative responses to injury and for successful axon regeneration. Efforts to improve functional outcomes by altering these pathways have yielded promising results in animal models of SCI, but neurological improvement remains limited.

The restricted success of such perturbations raises the possibility that neural plasticity and repair are tightly regulated mechanisms in vivo and that compensatory changes in response to experimental interventions might limit the benefit of any single gene or protein targeting strategy. With regard to cell-extrinsic inhibitory pathways, both CSPGs (18, 19) and Nogo-66 receptor 1 (NgR1) and paired Ig-like receptor B (PirB) ligands (20–22) have key roles in developmental restriction of critical period experience-dependent plasticity, and expression can be regulated by training (23). These pathways limit adult behavioral plasticity in multiple paradigms (22, 24). NgR1, NgR2, and PirB are neuronal receptors for the ligands NogoA, myelin-associated glycoprotein (MAG), and oligodendrocyte myelin glycoprotein (OMgp), which are produced by either oligodendrocytes or neurons (25–29). Both ligand blockade with the NgR1-Fc decoy receptor and *Ngr1* gene deletion result in improved neural repair, plasticity, and functional neurological recovery after traumatic SCI (11, 13–15, 30–33). However, the degree of axonal sprouting and regeneration is substantially greater with pharmacological intervention after injury, as opposed to constitutive genetic elimination. For example, *Ngr1* gene deletion allows functional recovery, corticospinal tract (CST) sprouting, and raphespinal regeneration but supports little or no CST regeneration after mid-thoracic dorsal hemisection (30, 33). In contrast, the CST regenerates after the same injury with delayed NgR1-Fc treatment, and functional recovery occurs even long after injury (15).

Gene expression profiling has been used extensively to evaluate mechanisms of axonal regeneration, comparing injury-induced expression in wild-type (WT) animals for different neuronal populations with robust or limited regenerative capacity. Such studies have described a set of genes with increased expression during successful peripheral nerve regeneration that fail to be induced by central injury. Such factors include growth-associated protein 43 (GAP-43), small proline-rich protein 1A (SPRR1A), activating transcription factor 3 (ATF3), and many others (34–38). The interaction between therapeutic interventions to promote neural repair and compensatory expression patterns limiting recovery has not been studied in any systematic fashion.

We initiated a study of SCI responses in *Ngr1*<sup>-/-</sup> mice. The *ORL1* mRNA, which encodes a seven-transmembrane domain G protein-coupled receptor for the opioid-related peptide

nociceptin (39), was induced selectively in SCI mice lacking NgR1. We observed protein interactions between ORL1 and NgR1, which facilitated the O- glycosylation and surface expression of NgR1. ORL1 abundance was inversely correlated with axonal regeneration in cortical neuron culture. Nociceptin/ORL1 signaling inhibited axon regeneration even when NgR1 was absent, indicating that ORL1 had NgR1-dependent and NgR1-independent functions. Antagonism of the ORL1 receptor after SCI resulted in greater neurological recovery and raphespinal axon growth. Thus, analysis of compensatory expression changes in *Ngr1*<sup>-/-</sup> mice with SCI identifies the nociceptin receptor ORL1 as a pharmacologically tractable approach to improving recovery after central nervous system (CNS) trauma.

## RESULTS

### NgR1 interacts with ORL1

To identify regulators of the NgR1 signaling pathway that might mediate compensatory limitation of regenerative responses in *Ngr1* null mice, we performed RNA microarray analysis using WT and *Ngr1*<sup>-/-</sup> mice brainstem 4 days after SCI. We used brainstem tissue for this study because SCI studies in *Ngr1*<sup>-/-</sup> mice showed raphespinal and rubrospinal axon regeneration, whereas the *Ngr1* null corticospinal regeneration phenotype was less pronounced (30, 33). There was increased *ORL1* [which encodes opioid receptor- like 1, nociceptin receptor (39)] mRNA expression in *Ngr1*<sup>-/-</sup> as compared to WT samples (Fig. 1A and table S1). To confirm this RNA microarray data, we performed quantitative polymerase chain reaction (qPCR) analysis. Compared to uninjured WT mice, *ORL1* mRNA expression was increased selectively in the brainstem but not in the cortex and cerebellum of *Ngr1*<sup>-/-</sup> mice subjected to mid-thoracic dorsal hemisection (fig. S1A). *ORL1* expression is increased in spinal cord tissue after peripheral sciatic nerve trauma in rats (40).

In human embryonic kidney–293T (HEK293T) cells, overexpressed NgR1 immunoprecipitates contained ORL1 and low-affinity nerve growth factor receptor (p75NTR), a binding partner for NgR1 (41), but not the control transmembrane protein neuropilin 1 (Fig. 1B and fig. S1B). Furthermore, association of endogenous NgR1 and ORL1 was detected in lysates from mouse forebrain and cultured hippocampal neurons (Fig. 1, C and D, and fig. S1, C and D). Next, we examined the subcellular localization of these proteins. In nonpermeabilized Cos7 cells, NgR1 colocalized with ORL1 at the cell surface (Fig. 1E). Thus, ORL1 is a binding partner of NgR1, and *ORL1* mRNA level is titrated by NgR1 after spinal cord trauma.

### ORL1 increases O-linked glycosylation of NgR1 in HEK293T cells

We noted that overexpressed NgR1 migrated by SDS–polyacrylamide gel electrophoresis (SDS-PAGE) as a doublet and that the more slowly migrating upper band was selectively increased by ORL1 coexpression (Fig. 1B). ORL1 over-expression dose-dependently enhanced the abundance of the more slowly migrating upper band for NgR1 but not that for NgR2 (Fig. 2A and fig. S2A), even though ORL1 associated with both NgR1 and NgR2 when over-expressed (fig. S2, B and C). Because NgRs are N- and O-linked glyco-proteins (42), we sought to clarify whether the band shift reflected differential NgR1 glycosylation using N- or O-glycosidase in NgR1-and ORL1-transfected HEK293T cells. N-glycosidase

treatment of lysates resulted in faster migration of both bands (Fig. 2B, and fig. S2, D and E). In contrast, O-glycosidase treatment of lysates reduced the levels of the upper band but not those of the lower bands, suggesting that the distinct mobilities of the bands might reflect differences in O-linked glycosylation. Consistent with this observation, inhibition of O-glycosylation by benzyl-*N*-acetyl- $\alpha$ -D-galactosaminide (GalNAc) dose-dependently reduced the upper band for NgR1 either without or with ORL1 overexpression (Fig. 2C, and fig. S2, F and G), as expected if the difference between the two bands reflected O-glycosylation of NgR1. O-linked glycosylation occurs in the Golgi apparatus (43–45), and both NgR1 and ORL1 colocalized with the Golgi body marker GM130 in permeabilized Cos7 cells (Fig. 2D). We conclude that expression of ORL1 increases O-linked glycosylation of NgR1.

### ORL1 increases the cell surface expression of NgR1

To function as an inhibitory receptor, NgR1 protein must undergo maturation and transport to the cell surface where NgR1 is present as a glycosylphosphatidylinositol (GPI)-linked protein, which can be released into the medium by phosphatidylinositol-specific phospholipase C (PI-PLC) (25). Treatment of NgR1-expressing HEK293T cells with PI-PLC decreased the amounts of the upper NgR1 band without altering those of the lower band (Fig. 3A, and fig. S3, A and B). Because ORL1 enhanced O-linked glycosylation and increased the abundance of the upper NgR1 band, whereas PI-PLC reduced only this form of NgR1, the data implied that ORL1 enhanced the surface expression of NgR1. Consistent with this notion, flow cytometry of a Cos7 cell line stably expressing FLAG-NgR1 showed that ectopic expression of ORL1 significantly increased the cell surface expression of NgR1 (Fig. 3, B and C).

ORL1 may increase the cell surface expression of NgR1 by altering the stability of the protein. To examine NgR1 half-life, we treated cells with cycloheximide (CHX) to block new protein synthesis and monitored the loss of preexisting NgR1. The levels of the upper NgR1 band peaked 3 hours after CHX treatment in control cells, whereas the timing of the maximum was shifted earlier, to 1 hour, in ORL1-expressing cells, consistent with more rapid glycosylation and maturation (Fig. 3, D and E). After 6 hours, the abundance of the upper NgR1 band in the ORL1-transfected cells remained higher than in the CHX-free control cells (0 hour). Thus, the upper bands for NgR1, which correspond to the O-glycosylated form, were more stable than the lower bands for NgR1, which correspond to the non-O-glycosylated form, regardless of the presence or absence of ORL1. These experiments demonstrate that ORL1 accelerates the O-linked glycosylation of NgR1 and increases the cell surface expression of NgR1.

### O-glycosylation is required for cell surface expression of NgR1

The amino acid sites for O-linked glycosylation in NgR1 have been predicted by mass spectrometry (46). To provide experimental evidence for those sites being necessary for O-linked glycosylation, we created single amino acid mutations of NgR1 in which alanine replaced serine or threonine, but observed only slight reductions of NgR1 glycosylation (fig. S4A). Because single sites can have weak effects, we generated multiple mutations of the proposed glycosylation sites. Although several double and triple amino acid substitutions

yielded little change in the intensity-modified upper NgR1 band, substitution of all seven predicted glycosylation sites (7xSA-TA) reduced NgR1 modification (fig. S4, B and C), suggesting that these seven amino acids are critical for O-linked glycosylation of NgR1. We used this 7xSA-TA mutant NgR1 to confirm the mechanism of ORL1-mediated regulation of NgR1. Cell surface expression of WT NgR1, but not that of 7xSA-TA NgR1, was increased in ORL1-expressing HEK293T cells (fig. S4D). This lack of ORL1 effect for 7xSA-TA NgR1 was not due to lack of protein interaction as determined by coimmunoprecipitation (fig. S4, E and F). Instead, we conclude that the ORL1 association with 7xSA-TA NgR1 did not increase surface expression because ORL1-enhanced O-glycosylation of mutant NgR1 was not possible.

### Knockdown of ORL1 decreases NgR1 protein in Neuro2A cells and primary neurons

We sought to extend our analysis of the ORL1/NgR1 interaction with loss-of-function experiments in the mouse neuroblastoma cell line Neuro2A, which expresses ORL1 endogenously. Endogenous NgR1 expression in Neuro2A cells is low, so we generated stable cell lines expressing FLAG-NgR1 (Neuro2A/FLAG-NgR1). In Neuro2A/FLAG-NgR1 cells, NgR1 migrated as a single band and more slowly than the immature NgR1 lower band lacking O-glycosyl groups in HEK293T cells (fig. S5A). The differential NgR1 processing between cell lines may reflect the different tissues of origin or expression levels. Knockdown of ORL1 (fig. S5, B to D) significantly reduced NgR1 protein levels in Neuro2A cells (Fig. 4, A and B). Although ORL1 selectively increased the abundance of the upper NgR1 band in HEK293T cells, ORL1 expression determined the total NgR1 level in Neuro2A cells. Thus, O-glycosylation may titrate NgR1 protein stability and levels in Neuro2A cells, and ORL1 knockdown reduces O-glycosylation to restrict NgR1 accumulation. The specificity of the small interfering RNA (siRNA) effect was confirmed by rescue with an siRNA-insensitive expression vector for human ORL1 (fig. S5, E and F). Flow cytometry confirmed that the surface abundance of NgR1 was significantly decreased in ORL1 knockdown cells compared to control cells (Fig. 4, C and D). NgR1 is abundant in cortical neurons, and lentiviral transduction of short hairpin RNAs (shRNAs) targeting ORL1 into cortical neurons (fig. S5G) reduced the protein abundance of NgR1 (Fig. 4, E and F) without affecting its mRNA expression (fig. S5H), demonstrating that ORL1 regulation of NgR1 abundance occurs post-transcriptionally. In contrast, overexpressed ORL1 increased NgR1 protein level in these neurons (Fig. 4, G and H), consistent with the augmented NgR1 maturation by ORL1 protein expression.

We used benzyl-GalNAc to inhibit O-linked glycosylation in primary neurons. NgR1 expression in cortical neurons was decreased by benzyl-GalNAc treatment (Fig. 4I and fig. S5I). To check the surface expression of NgR1 protein, primary neurons were incubated with PI-PLC, and the culture medium was immunoprecipitated for NgR1 (Fig. 4J, and fig. S5, J to L). NgR1 levels were significantly decreased in the lysate but increased in culture medium after PI-PLC treatment. Then, we analyzed NgR1 protein levels in culture medium after PI-PLC treatment of benzyl-GalNAc-exposed neurons. As expected, inhibition of O-glycosylation decreased the surface expression of NgR1 in culture neurons (Fig. 4K and fig. S5M). To ensure that these changes were consistent with the rate of new NgR1 protein synthesis, we assessed the NgR1 protein turnover using CHX in culture neurons. Blockade

of protein synthesis resulted in a significant reduction of total NgR1 protein after 24 hours of CHX treatment of cortical neurons (Fig. 4L and fig. S5N). Using NgR1 protein levels in PI-PLC– treated culture medium as a measure of neuronal surface NgR1, we observed a similar decrease within 24 hours of CHX treatment (Fig. 4M and fig. S5O). Thus, inhibition of O-glycosylation and NgR1 maturation reduced steady-state surface levels of NgR1 by preventing the delivery of new NgR1 protein to the cell surface.

### Loss of ORL1 enhances axon regeneration in the presence of Nogo

Nogo22, a C-terminal portion of NogoA that includes the Nogo66 domain, binds to NgR1 and suppresses regeneration of cortical axons in vitro after traumatic disruption (27). We reasoned that altered surface NgR1 levels may modify the sensitivity of neuronal repair to NogoA-induced inhibition. In vitro regeneration of shORL1-treated neurons in the presence of Nogo22 was similar to that of control neurons without Nogo22 (Fig. 5, A and B). However, Nogo22 still attenuated regeneration in neurons with ORL1 knockdown (Fig. 5B). The residual inhibition of regeneration by the Nogo ligand may relate to the limited 30 to 40% reduction of NgR1 expression caused by 60 to 70% ORL1 knockdown (Fig. 4, E and F, and fig. S5G). Consistent with this observation, *Ngr1*<sup>+/-</sup> mice do not exhibit gene dosage effects relative to *Ngr1*<sup>+/+</sup> and *Ngr1*<sup>-/-</sup> mice (30). Unexpectedly, we observed that ORL1 knockdown neurons consistently showed greater basal regeneration in the absence of Nogo-22 than short- hairpin nontargeting control (shNC)–treated neurons (Fig. 5B).

### ORL1/nociceptin signaling directly inhibits axon regeneration

Because reduction of ORL1 expression resulted in enhanced axon regeneration, ORL1 signaling itself may play a role in neural repair after trauma, separately from the NogoA/ NgR1 axis. Consistent with this notion, the extent of facilitation of axon regeneration by ORL1 knockdown was similar for WT and *Ngr1*<sup>-/-</sup> neurons (Fig. 5, C and D). Conversely, overexpression of ORL1 inhibited axonal regeneration independently of NgR1 (Fig. 5, E and F). Thus, loss- and gain-of-function data suggest that ORL1 expression regulates axon regeneration independently of NgR1, in addition to modulating NgR1 levels. Next, we examined the influence of the ORL1 agonist nociceptin on axonal growth after injury. Nociceptin suppressed axon regeneration dose dependently in WT neurons and in *Ngr1*<sup>-/-</sup> neurons (Fig. 6, A and B). The nonpeptidic ORL1 antagonist J113397 selectively blocks nociceptin/ORL1 signaling in vitro and in vivo (47, 48) and enhanced axonal regeneration (Fig. 6, C and D). Furthermore, nociceptin-mediated inhibition of axon growth was reduced in the presence of J113397 (fig. S6, A and B). Despite the effect of ORL1 expression on NgR1 protein level, ORL1 activation modulation with nociceptin or J113397 did not change NgR1 levels (fig. S6, C to F). Moreover, the additive effects of combined treatment with Nogo22 and nociceptin (Fig. 6, E and F) or Nogo and J113397 (fig. S6, G and H) were consistent with the independent action of each intervention on regeneration. Thus, the ability of nociceptin/ORL1 signaling and Nogo/NgR1 signaling to regulate axon regeneration in these cultures appears to be separate from one another.

### ORL1/nociceptin inhibition of regeneration requires Rho/ROCK signaling

In other cell types, nociceptin/ORL1 signaling can activate RhoA and Rho-associated kinase (ROCK) signaling to alter the F-actin cytoskeleton (49, 50). Because the Rho pathway is

implicated in axonal growth inhibition by several ligands, including Nogo and CSPG (51–53), we considered its necessity for nociceptin inhibition of axonal regeneration. The ROCK inhibitor Y27632 enhanced regeneration and prevented inhibition of this process by nociceptin (Fig. 6, G and H). Thus, both Nogo and nociception inhibition of axon regeneration are mediated through Rho/ROCK signaling.

### The ORL1 antagonist J113397 improves recovery from traumatic SCI

Because ORL1 antagonism enhanced axonal repair in vitro, we sought to determine whether J113397 enhanced functional recovery from traumatic SCI. WT mice received dorsal hemisection of the midthoracic spinal cord and were randomized to receive either J113397 (0.2 mg/kg per day) (54) or an equal volume of saline by daily subcutaneous injection, starting on day 5 and continuing through day 56 after injury. The Basso Mouse Scale (BMS) score, which measures open-field locomotion and is rated on a scale from 0 to 9 (55), was significantly improved in J113397-treated animals compared with the vehicle group between 6 and 10 weeks after axotomy (Fig. 7A). The temporal pattern was consistent with enhanced neural repair and not a symptomatic effect of J113397, because there was no benefit during the first 3 weeks of treatment (Fig. 7A) and because the benefit was not lost during a 2-week drug washout period after treatment (Fig. 7A). The BMS subscore discriminates fine differences in stepping frequency, coordination, paw position, trunk stability, and tail position. There was a nonsignificant trend toward improved BMS subscore for J113397-treated animals from 6 to 8 weeks (fig. S7A). The J113397 group also exhibited a nonsignificant improvement trend in both the rotarod test and Gridwalk analysis at day 56 after injury (fig. S7, B and C). These behavioral differences were not due to differences in the degree of injury or in tissue sparing, because intact tissue was identical in the two groups as assessed by glial fibrillary acidic protein (GFAP) immunohistochemistry at the end of the experiment (Fig. 7B). Although the standard dose of J113397 (in vitro, 10 nM; in vivo, 0.2 mg/kg per day) (54) increased axonal regeneration or improved behavior, a substantially higher dose (in vitro, 100 and 500 nM; in vivo, 2 mg/kg per day) suppressed regeneration in vitro (fig. S8A) and exhibited a nonsignificant trend toward impaired outcomes in vivo (fig. S8, B and C).

Because combined treatment with Nogo22 and nociceptin yielded an additive effect on regeneration (Fig. 6F), and knockout of NgR1 increased *ORL1* expression after SCI (Fig. 1A), we hypothesized that the administration of J113397 to *Ngr1*<sup>-/-</sup> animals might enhance functional recovery after SCI. We used a more severe lesion for the combination experiments to avoid a ceiling effect for dual intervention. WT and *Ngr1*<sup>-/-</sup> animals were overhemisected and administered vehicle or J113397 (0.2 mg/kg per day) by subcutaneous injection, starting on day 3 until day 70 after injury, with washout of the drug until day 98. As determined by the BMS score, J113397-injected *Ngr1*<sup>-/-</sup> mice showed significant improvement in motor function compared to either WT mice injected with vehicle or with J113397 (Fig. 7C). In this more severe overhemisection setting, J113397 alone showed only a nonsignificant trend to greater recovery. The percentage of spared tissue was comparable among the groups (Fig. 7D), and all were less than the standard hemisection model used for the initial J113397 study (Fig. 7B). There was no significant improvement in J113397-injected WT mice in this severe injury cohort. The Grid-walk test, which evaluates skilled

locomotor function by counting foot faults as mice traverse a metal grid, revealed that J113397-treated *Ngr1*<sup>-/-</sup> mice achieved significantly enhanced functional recovery compared to WT groups (Fig. 7E). These data demonstrate that ORL1 antagonist treatment of *Ngr1*<sup>-/-</sup> mice generates greater recovery after SCI.

### ORL1 antagonist J113397 promotes raphespinal fiber growth in caudal spinal cord after SCI

Because of the in vitro regenerative effect of J113397 and the improved BMS scores, we looked for evidence for axonal growth after injury. We focused on the raphespinal system, which contributes substantially to locomotion and is significantly lesioned by the dorsal hemisection injury. Rostral to the lesion site, the density of 5HT+ terminals in the ventral horn of the cervical cord did not differ between vehicle and J113397 in WT groups on day 72 after dorsal hemisection injury (Fig. 8, A and B). The density of ventral horn 5HT+ terminals in lumbar enlargement was two times greater in the J113397 group compared to vehicle (Fig. 8, C and D). In addition, the density of 5HT+ terminals rostral to the lesion site was similar between WT and *Ngr1*<sup>-/-</sup> animals treated with J113397 after severe overhemisected injury (Fig. 8, E and F). Caudal to the lesion site, the 5HT+ density between vehicle and J113397 drug in the severe injury study did not differ between WT and *Ngr1*<sup>-/-</sup> mice. The density of ventral horn 5HT+ terminals in lumbar enlargement was significantly increased in *Ngr1*<sup>-/-</sup> mice, regardless of whether they received J113397, compared to WT groups (Fig. 8, G and H). Together, these results demonstrate that administration of the ORL1 antagonist J113397 after hemisection SCI in WT mice increased raphespinal axon sprouting caudal to injury site. The *Ngr1*<sup>-/-</sup> animals showed increased raphespinal axon sprouting in severe overhemisection studies. However, treatment of severely injured WT or *Ngr1*<sup>-/-</sup> mice with J113397 did not alter 5HT anatomy relative to vehicle. Although J113397 enhanced behavioral outcomes for severely injured *Ngr1*<sup>-/-</sup> mice (Fig. 7, C and E), this appears to occur independently of enhanced caudal 5HT axon regrowth (Fig. 8H) and is presumably mediated through other axon tracts not studied here.

## DISCUSSION

The current study showed that nociceptin/ ORL1 signaling limits neural repair. The identification of ORL1 as a brake on repair stemmed from the analysis of gene expression compensation after *NgR1* deletion, but was also supported by direct protein interactions of ORL1 with NgR1. ORL1 expression promoted glycosylation and surface expression of NgR1 to mediate inhibition of axonal regeneration by myelin-associated inhibitors. Moreover, data obtained from cultured neurons showed that nociceptin/ORL1 signaling through the RhoA/ROCK pathway inhibited axonal regeneration independently of NgR1. Treatment with an ORL1 antagonist in a clinically relevant time window enhanced neural repair and recovery of mice after SCI. The multiple interactions of nociceptin/ORL1 signaling with NgR1 signaling in the control of neural repair after trauma are illustrated in fig. S9.

Although several specific cell-intrinsic and cell-extrinsic factors limiting neural repair after traumatic SCI have been identified by various methods, manipulating these factors only



partially improves neurological recovery in vivo. We hypothesized that axonal growth and sprouting in the adult CNS might be tightly regulated by multiple redundant mechanisms. Therefore, the benefit of growth-promoting perturbations might be limited by compensatory gene expression changes. We searched for altered gene expression after SCI in mice lacking an inhibitor of neural repair NgR1. Although the general pattern of gene expression after axotomy has been studied in several control situations (34–38), the variation in such patterns after a growth inhibitory pathway has been deleted and has not been a major area of study (56). From this analysis, we focused on *ORL1*, which is altered by SCI trauma only in the absence of NgR1, and not by either axotomy or *Ngr1* deletion alone. This approach has the potential to identify a gene induced in a compensatory manner to limit adult axonal growth after injury when one endogenous brake is removed. This appears to be the case for *ORL1*.

Whether the *ORL1* gene is induced only by SCI in combination with *Ngr1* deficiency is not clear. Future experiments will assess whether other forms of injury, such as ischemic stroke, in the absence of NgR1 yield similar increases in *ORL1* expression and whether SCI with suppression of other pathways, such as CSPG or PTEN, might also result in increased *ORL1* expression. The mechanism of increased *ORL1* transcriptional regulation is not defined here but may involve responsiveness to trauma-induced axonal sprouting mediated by *Ngr1* deletion. *ORL1* appears to limit such axonal sprouting and, hence, neurological recovery.

*ORL1* and NgR1 interacted posttranslationally and at the transcriptional level. Overexpressed and endogenous forms of these two proteins associated with one another. This interaction increased O-linked glycosylation and cell surface expression of NgR1 without altering transcription. In NgR1-overexpressing nonneuronal cells, immature forms of NgR1 protein accumulated intracellularly, but *ORL1* accelerated maturation and glycosylation. In neuronal cells, only mature O-glycosylated NgR1 was detected, and *ORL1* coexpression increased the surface level of mature NgR1. The interaction of *ORL1* with NgR1 did not require the serine/threonine residues subject to O-linked glycosylation, but regulated the modification of these residues by cellular enzymes. This may occur either directly by *ORL1* association with enzymatic components or indirectly by altered subcellular compartmentalization. We demonstrated that glycosylation was coupled with the delivery of NgR1 to the cell surface, and it is possible that O-linked glycosylation enhanced NgR1 stability. Consistent with an intracellular role for *ORL1*/NgR1 interactions, the addition of extracellular *ORL1* ligand did not alter NgR1 processing. The two proteins may be transported to the cell surface in a complex. Together, the data demonstrate a complex interplay between *ORL1* and NgR1 at the protein and RNA levels (fig. S9).

The ability of *ORL1* levels to alter NgR1 protein at the cell surface provides a mechanism for modification of neural repair. However, the *ORL1*/nociceptin axis also regulated axon regeneration separately from NgR1. *ORL1* overexpression reduced and knockdown-enhanced regeneration of cortical neurons, effects that occurred without addition of the *ORL1* ligand, so it may be mediated by ligand-independent action of the receptor (57) or by low levels of nociceptin in the culture system. In addition, ligand-dependent *ORL1* receptor agonism also determined axonal regeneration success. The *ORL1* agonist nociceptin dose-dependently inhibited regeneration, whereas the antagonist J113397 increased outgrowth above control levels. Because substantially higher concentrations of J113397 had negative

effects in vitro and in vivo, there may be either off-target actions at high concentrations or the response may be biphasic, increasing regeneration at low receptor occupancy and decreasing regeneration at higher occupancy. The current data define nociceptin/ORL1 signaling as an inhibitor of axonal regeneration.

ORL1 is a G protein-coupled receptor that can inhibit adenylate cyclase through  $G_i$  (58) and activate RhoA through  $G_{12/13}$  (49, 50). The RhoA/ROCK signaling pathway is implicated in the inhibition of axonal growth by multiple inhibitors including Nogo, MAG, myelin, CSPG, and repulsive guidance molecule BMP co-receptor a (RGMA) (53, 59). Similarly, the ROCK inhibitor Y27632 fully blocked inhibition of axonal regeneration by nociceptin. Thus, RhoA/ROCK signaling is a convergent point for these axonal growth inhibitors.

We assessed the ability of nociceptin antagonist J113397 to alter SCI outcomes when given 5 days after injury and observed improved motor recovery from mid-thoracic hemisection injury. The functional benefit was coupled with greater density of raphespinal innervation in the lumbar spinal cord without differences in lesion site severity. The increased 5HT density is likely due to a combination of axonal sprouting and regeneration in the presence of ORL1 blockade by J113397. The serotonergic system participates in loco-motor function (15, 30, 32, 60), so this J113397-induced raphespinal growth likely contributes to the improved outcome. However, because ORL1 expression is widespread, it is likely that J113397 improves treatment by affecting multiple pathways, and no single pathway is the proximate cause for functional improvements.

The increased ORL1 abundance in *Ngr1*<sup>-/-</sup> mice provided a rationale for combining ORL1 and NgR1 antagonism. After a severe SCI, there was an additive benefit of deleting the *NgR1* gene and pharmacologically blocking ORL1. The additive benefit was prominent for behavioral tests but not detected when scoring raphespinal fiber density, which was increased by *NgR1* deletion alone. We hypothesize that the anatomical repair of other fiber systems responds additively to dual inhibition.

As mentioned above, ORL1 may also play a role in limiting repair when other inhibitory pathways are blocked. Examination of expression changes of injured neurons in which one inhibitory pathway is deleted, as opposed to injury in WT mice, has uncovered a regeneration-regulating pathway. It seems likely that studying compensatory expression patterns after blockade of other inhibitory pathways will uncover additional regeneration pathways not readily detectable in WT mice with or without injury.

## MATERIALS AND METHODS

### Cell lines and primary cortical neuron culture

HEK293T, African green monkey kidney Cos7, and mouse neuroblastoma Neuro2A cells were maintained in Dulbecco's modified Eagle's medium containing 10% fetal bovine serum, penicillin (100 U/ml), and streptomycin (100 µg/ml). Stable Cos7 and Neuro2A cells overexpressing FLAG-NgR1 were generated and maintained in the above medium with G418 (0.5 mg/ml). Briefly, cells were transfected with the p3XFLAG-CMV-NgR1 construct, and single-cell clones were established by a limiting dilution technique. Mouse E17 cortical

neurons were cultured in Neurobasal-A media supplemented with B-27, GultaMAX, and penicillin-streptomycin (all from Invitrogen) on tissue culture plates coated with poly-D-lysine.

### Expression plasmids, antibodies, and reagents

WT human NgR1 (61) was subcloned into p3xFLAG-CMV9 vector and used for generating mutant constructs by PCR methods using KOD Hot start DNA polymerase (Toyobo) and sequenced. Hemagglutinin (HA)-neuropilin (62), Myc-NgR1 (25), and Myc-NgR2 (63) have been previously described. HA-tagged human ORL1 construct was obtained from UMR cDNA Resource Center. Anti-ORL1 rabbit serum was a gift from J. Hamid, University of Calgary (64). Anti-FLAG (#F7425 or #F3165), anti-HA (#H9658 or #H6908), anti-Myc (#M4439 or #C3956), anti-GFAP (#G3893), and anti- $\beta$ -actin (#A1978) antibodies (all from Sigma-Aldrich), anti-NgR1 (#AF1440) and anti-NgR2 (#AF2776) antibodies (R&D Systems), anti-ORL1 antibody (#RA14140, Neuromics), anti- $\beta$ III-tubulin antibody (#G7121, Promega), anti-5-hydroxytryptamine (5HT) antibody (#20080, ImmunoStar), and anti-GM130 antibody (#610823, BD Transduction Laboratories) were used for the following experiments. PI-PLC was from Sigma- Aldrich, CHX was from Wako, benzyl-GalNAc and nociceptin were from Calbiochem, and ( $\pm$ )-J113397 was purchased from Tocris Bioscience. Nogo22 protein has been described previously (27).

### Transfection and transduction

Plasmids were transfected into HEK293T and Cos7 cells with Lipofectamine 2000 (Invitrogen) and into Neuro2A cells with X-tremeGENE (Roche). Neuro2A cells were transfected with siRNA NC [rCrGrU-rUrArArUrCrGrCrGrUrArUrArArUrArCrGrCrUrUAT (sense) and rArUrArCrGrCrGrUrArUrArUrArCrGrCrGrArUrUrArAr-CrGrArC (antisense)] or targeting mouse ORL1 [#1, rGrCrArAr-GrArCrGrGrUrCrArUrUrGrCrUrArUrCrGrArCTA (sense) and rUrArGrUrCrGrArUrArGrCrArArUrGrArCrCrGrUrCrUrUrGr-CrArC (antisense); #2, rCrUrGrCrUrArCrArGrCrCrUrCrArUrGrArUrUrCrGrArCGA (sense) and rUrCrGrUrCrGrArArUrCrArUrGr-A rGrGrCrUrGrUrArGrCrArGrArC (antisense)] using Lipofectamine RNAiMAX (Invitrogen). Cortical neurons were transfected with pcDNA3 vector or HA-ORL1 plasmid using the Amaxa Mouse Neuron Nucleofector kit (Lonza), or lentivirally transduced with shRNA targeting control (catalog #SHC002V, Sigma-Aldrich) or mouse ORL1 (#1 TRCN0000027784 and #2 TRCN0000027850, Sigma-Aldrich).

### Immunoprecipitation and immunoblotting

Cells were lysed with a radioimmunoprecipitation assay (RIPA) buffer [50 mM tris-HCl (pH 7.4), 150 mM NaCl, 1 mM EDTA, 0.1% SDS, 0.5% sodium deoxycholate, and 1% Triton X-100) and centrifuged at 20,000g for 20 min at 4°C. Mouse forebrain was homogenized in RIPA buffer, and the extracts were centrifuged at 20,000g for 30 min. Antibody and protein G-sepharose mixture were added to supernatants and incubated for 2 hours at 4°C with gentle rotation. The beads were washed three times, and the immune complexes were then resolved by SDS-PAGE. After transfer, nitrocellulose membranes were incubated in blocking buffer (Blocking Buffer for Fluorescent Western Blotting, Rockland MB-070-010) for 1 hour at room temperature (RT) and immunoblotted with the appropriate primary

antibodies. After primary antibody incubation, secondary antibodies (Odyssey IRDye 680 or 800) were applied for 1 hour at RT. Membranes were then washed and visualized using a LiCor Odyssey Infrared Imaging System.

### Immunocytochemistry

At 36 hours after transfection, Cos7 cells expressing FLAG-NgR1 and HA-ORL1 were fixed with 4% paraformaldehyde for 15 min and then permeabilized with 0.1% Triton X-100 in phosphate-buffered saline (PBS) for 15 min. The samples were incubated overnight at 4°C with anti-FLAG (1:1000) and anti-HA (1:1000), or anti-NgR1 (1:1000), anti-HA (1:1000), and anti-GM130 (1:500) antibodies. Then, either Alexa 488–conjugated donkey anti-mouse immunoglobulin G (IgG) and Alexa 568–conjugated donkey anti-rabbit IgG, or Alexa 488–conjugated donkey anti-goat IgG, Alexa 568–conjugated donkey anti-rabbit IgG, and Alexa 647–conjugated donkey anti-mouse IgG (1:2000; all from Invitrogen) were used to detect primary antibodies. Samples were mounted with mounting solution (Vector Laboratories) and observed using an LSM710 confocal microscope.

### Glycosidase digestion

Cell lysates were denatured using denaturing buffer (New England BioLabs) for 10 min at 95°C and then subjected to digestion with N-Glycosidase F (Calbiochem) or O-Glycosidase and neuraminidase (New England BioLabs) for 2 hours at 37°C as directed by the manufacturer. The samples were then subjected to SDS-PAGE for immunoblots.

### PI-PLC treatment

GPI-anchored proteins were released from cultured cells by PI-PLC (Sigma-Aldrich) treatment. To generate cell lysates for Western blot analysis, cells were treated with PI-PLC (0.05 or 0.5 U/ml) at 37°C for 1 hour before lysis. To analyze released proteins from the cell surface, culture medium was replaced with PI-PLC–containing medium (1 U/ml) and incubated at 37°C for 1 hour. The culture medium was then centrifuged at 5000g for 10 min at 4°C. The supernatant was immunoprecipitated with anti-NgR1 antibody and protein G–sepharose mixture and incubated for 2 hours at 4°C with gentle rotation. The beads were washed three times, and the immune complexes were resolved by SDS-PAGE.

### Flow cytometry

Cells were fixed with 4% formaldehyde for 15 min, washed with PBS three times, and trypsinized to obtain cell suspension. After three washes, cells were incubated in anti-FLAG (1:500) antibody for 1 hour and then subsequently incubated in Alexa 488–conjugated anti-mouse IgG antibody (1:1000) for 1 hour. Cell surface NgR1 protein levels were measured using a FACSCalibur flow cytometer (BD Biosciences) and analyzed by using CellQuest software.

### Reverse transcription PCR and qPCR

Total RNA was prepared using TRIzol (Sigma-Aldrich) and subjected to reverse transcription PCR using the M-MuLV Reverse Transcriptase (New England BioLabs). cDNAs were used for real-time qPCR with iQ supermix (Bio-Rad) and TaqMan Gene

Expression Assay (#Mm00452228 for mNgR1, #Mm00440563 for mORL1, and #Mm03302249 for Gapdh from Applied Biosystems) on a Bio-Rad CFX Connect Real-Time PCR Detection System using standard cycles. Each sample was analyzed in triplicate.

### Cortical axon regeneration assay (cortical scrape assay)

Scrape assay was performed as described previously (27). Primary cortical cultures were established from E17 C57BL/6 mice. Digested cells were plated on 96-well poly-D-lysine-coated plates at a density of 25,000 cells per well in 200  $\mu$ l of plating medium. For knockdown experiments, lentiviral particles for shRNA control or targeting mORL1 clones as described above were added at 3 days in vitro (DIV). On 8 DIV, 96-well cultures were scraped using a custom-fabricated 96-pin array, and vehicle and/or the indicated amount of Nogo22, nociceptin, or J113397 were added. Neurons were allowed to regenerate for another 72 hours before fixing with 4% paraformaldehyde. Regenerating axons in the scrape zone were visualized using an antibody against  $\beta$ III-tubulin (1:2000). Growth cones were visualized by staining for F-actin using rhodamine-conjugated phalloidin (1:2000; #R415, Life Technologies). Cell density was visualized using the nuclear marker 4',6-diamidino-2-phenylindole (0.1  $\mu$ g/ml, #4083; Cell Signaling Technology). Images were taken on a 10 $\times$  objective in an automated high-throughput imager (ImageXpress Micro XLS, Molecular Devices) under identical conditions. Regeneration zone identification, image thresholding, and quantitation were performed using a MATLAB script (65).

### Mice, surgery, and behavioral test

The *Ngr1*<sup>-/-</sup> mouse line has been described (30) and were back-crossed for more than nine generations to C57BL/6 WT (*Ngr1*<sup>+/+</sup>) mice. Primary neuron cultures were obtained from these mice. Age-matched adult (10 weeks) WT female mice were subjected to dorsal hemisection as described previously (65). Animals received sub-cutaneous injection of buprenex (0.01 mg/kg) 30 min before surgery and were deeply anesthetized with ketamine (100 mg/kg) and xylazine (15 mg/kg). To expose the dorsal spinal cord at the T6 and T7 levels, laminectomy was performed. Dura mater was pierced and 1% lidocaine was dropped on the exposed cord for 1 min. A pair of microscissors was used to lesion the spinal cord to a depth of 1.0 mm (hemisection for drug study in WT animals) or 1.2 mm (overhemisection for the WT and *Ngr1*<sup>-/-</sup> cohort) to completely sever the dorsal and dorso-lateral CST. The lateral aspect of the spinal cord was scraped with a 30-gauge needle to ensure completeness of the lesion. Muscle and skin overlying the lesion were sutured. Animals received subcutaneous injections of ampicillin (100 mg/kg) and buprenex (0.1 mg/kg) twice a day for the first 2 days after surgery and additional injections as necessary. Injured animals were subcutaneously injected with either J113397 (0.2 mg/kg per day) or an equal volume of saline. Procedures and postoperative care were performed in accordance with the guidelines of the Institutional Animal Use and Care Committee at Yale University. An experimenter blinded to the treatment completed behavioral assessment. We used the BMS as a measure of open-field locomotion (55). Animals were tested 3 days before dorsal hemisection for baseline function; 3, 7, 14, 21, 28, 35, 42, 49, 56, 63, and 70 days post lesion (dpl) for hemisection; and 3, 7, 14, 21, 28, 35, 42, 49, 56, 63, 70, 77, 84, 91, and 98 dpl for overhemisection.

## Histology and immunohistochemistry

Mice were euthanized and transcardially perfused with cold PBS followed by 4% paraformaldehyde. Spinal cords were dissected, postfixed in 4% paraformaldehyde at 4°C, and embedded in 10% gelatin. Serial sections (40 µm) were collected on a vibratome (VT1000S, Leica). Transverse sections were collected at cervical enlargements and lumbar enlargements. The thoracic lesion site (from –5 mm rostral to +5 mm caudal) was excised from each animal and sectioned sagittally, and every single section was collected. Sections of spinal cord were blocked and permeabilized with 10% normal donkey serum and 0.3% Triton X-100 in PBS for 1 hour. Sections were incubated with anti-5HT (1:1000) or anti-GFAP (1:1000) antibody and visualized with Alexa 488–conjugated secondary antibody (1:1000). The images were analyzed by using National Institutes of Health ImageJ version 1.49, as described previously (11). For analysis of serotonin innervation, immunoreactive serotonin fibers in the ventral horn of transverse sections were selected by thresholding, and then the intensity of serotonin fiber per area was measured after using the “skeletonize” function.

## Additional behaviors

The rotarod test (56 dpl) for hemisected animal was used as a measure of motor coordination. The rotarod apparatus (Columbus Instruments) was set at a baseline speed of 2 rpm, with acceleration at 0.2 rpm/s. Latency for the animal to fall off the rotating drum was recorded. The average time was calculated from five consecutive trials in each session. Grid walking test (57 dpl for hemisected and 80 dpl for overhemisected animal) was performed previously (66). Mice were placed on an elevated 400-mm × 400-mm metal grid with 10-mm × 10-mm square space and allowed to freely explore the grid for 3 min. Mice were videotaped by reflection from a mirror placed under the grid and scored for the percentage of impaired steps out of the first 50 steps taken with left and right hind limbs individually. Impaired steps were scored when the limb fell between the rungs, when an incorrectly placed step occurred such that either the ankle or toes were placed on the rungs without proper grasping, or when the limb was correctly placed but slipped off during weight bearing.

## Statistics

Statistical comparisons using SPSS or Prism software included oneway analysis of variance (ANOVA) with post hoc Tukey’s pairwise comparisons, one-way ANOVA with post hoc Dunnett’s when comparing across a dose response to control values, repeated-measures ANOVA across SCI time series, and Student’s *t* test as specified in the figure legends. The assumption of normality for *t* tests was confirmed with the D’Agostino and Pearson test.

## Supplementary Material

Refer to Web version on PubMed Central for supplementary material.

## Acknowledgments:

We thank Y. Fu for the technical assistance.

## Funding:

This work was supported by grants from the NIH and Falk Medical Research Trust to S.M.S.

## REFERENCES AND NOTES

1. Park KK, Liu K, Hu Y, Smith PD, Wang C, Cai B, Xu B, Connolly L, Kramvis I, Sahin M, He Z, Promoting axon regeneration in the adult CNS by modulation of the PTEN/mTOR pathway. *Science* 322, 963–966 (2008). [PubMed: 18988856]
2. Liu K, Lu Y, Lee JK, Samara R, Willenberg R, Sears-Kraxberger I, Tedeschi A, Park KK, Jin D, Cai B, Xu B, Connolly L, Steward O, Zheng B, He Z, PTEN deletion enhances the regenerative ability of adult corticospinal neurons. *Nat. Neurosci* 13, 1075–1081 (2010). [PubMed: 20694004]
3. Moore DL, Blackmore MG, Hu Y, Kaestner KH, Bixby JL, Lemmon VP, Goldberg JL, KLF family members regulate intrinsic axon regeneration ability. *Science* 326, 298–301 (2009). [PubMed: 19815778]
4. Sun F, Park KK, Belin S, Wang D, Lu T, Chen G, Zhang K, Yeung C, Feng G, Yankner BA, He Z, Sustained axon regeneration induced by co-deletion of PTEN and SOCS3. *Nature* 480, 372–375 (2011). [PubMed: 22056987]
5. Bradbury EJ, Moon LDF, Popat RJ, King VR, Bennett GS, Patel PN, Fawcett JW, McMahon SB, Chondroitinase ABC promotes functional recovery after spinal cord injury. *Nature* 416, 636–640 (2002). [PubMed: 11948352]
6. Alilain WJ, Horn KP, Hu H, Dick TE, Silver J, Functional regeneration of respiratory pathways after spinal cord injury. *Nature* 475, 196–200 (2011). [PubMed: 21753849]
7. Chen MS, Huber AB, van der Haar ME, Frank M, Schnell L, Spillmann AA, Christ F, Schwab ME, Nogo-A is a myelin-associated neurite outgrowth inhibitor and an antigen for monoclonal antibody IN-1. *Nature* 403, 434–439 (2000). [PubMed: 10667796]
8. GrandPré T, Nakamura F, Vartanian T, Strittmatter SM, Identification of the Nogo inhibitor of axon regeneration as a Reticulon protein. *Nature* 403, 439–444 (2000). [PubMed: 10667797]
9. Mukhopadhyay G, Doherty P, Walsh FS, Crocker PR, Filbin MT, A novel role for myelin-associated glycoprotein as an inhibitor of axonal regeneration. *Neuron* 13, 757–767 (1994). [PubMed: 7522484]
10. Wang KC, Koprivica V, Kim JA, Sivasankaran R, Guo Y, Neve RL, He Z, Oligodendrocyte-myelin glycoprotein is a Nogo receptor ligand that inhibits neurite outgrowth. *Nature* 417, 941–944 (2002). [PubMed: 12068310]
11. Wang X, Yigitkanli K, Kim C-Y, Sekine-Komo T, Wirak D, Frieden E, Bhargava A, Maynard G, Cafferty WBJ, Strittmatter SM, Human NgR-Fc decoy protein via lumbar intrathecal bolus administration enhances recovery from rat spinal cord contusion. *J. Neurotrauma* 31, 1955–1966 (2014). [PubMed: 24964223]
12. Schwab ME, Strittmatter SM, Nogo limits neural plasticity and recovery from injury. *Curr. Opin. Neurobiol* 27, 53–60 (2014). [PubMed: 24632308]
13. Wang X, Duffy P, McGee AW, Hasan O, Gould G, Tu N, Harel NY, Huang Y, Carson RE, Weinzimmer D, Ropchan J, Benowitz LI, Cafferty WBJ, Strittmatter SM, Recovery from chronic spinal cord contusion after Nogo receptor intervention. *Ann. Neurol* 70, 805–821 (2011). [PubMed: 22162062]
14. Wang X, Baughman KW, Basso DM, Strittmatter SM, Delayed Nogo receptor therapy improves recovery from spinal cord contusion. *Ann. Neurol* 60, 540–549 (2006). [PubMed: 16958113]
15. Li S, Liu BP, Budel S, Li M, Ji B, Walus L, Li W, Jirik A, Rabacchi S, Choi E, Worley D, Sah DWY, Pepinsky B, Lee D, Relton J, Strittmatter SM, Blockade of Nogo-66, myelin-associated glycoprotein, and oligodendrocyte myelin glycoprotein by soluble Nogo-66 receptor promotes axonal sprouting and recovery after spinal injury. *J. Neurosci* 24, 10511–10520 (2004). [PubMed: 15548666]
16. Hammarlund M, Nix P, Hauth L, Jorgensen EM, Bastiani M, Axon regeneration requires a conserved MAP kinase pathway. *Science* 323, 802–806 (2009). [PubMed: 19164707]

17. Watkins TA, Wang B, Huntwork-Rodriguez S, Yang J, Jiang Z, Eastham-Anderson J, Modrusan Z, Kaminker JS, Tessier-Lavigne M, Lewcock JW, DLK initiates a transcriptional program that couples apoptotic and regenerative responses to axonal injury. *Proc. Natl. Acad. Sci. U.S.A* 110, 4039–4044 (2013). [PubMed: 23431164]
18. Pizzorusso T, Medini P, Berardi N, Chierzi S, Fawcett JW, Maffei L, Reactivation of ocular dominance plasticity in the adult visual cortex. *Science* 298, 1248–1251 (2002). [PubMed: 12424383]
19. Gogolla N, Caroni P, Lüthi A, Herry C, Perineuronal nets protect fear memories from erasure. *Science* 325, 1258–1261 (2009). [PubMed: 19729657]
20. McGee AW, Yang Y, Fischer QS, Daw NW, Strittmatter SM, Experience-driven plasticity of visual cortex limited by myelin and Nogo receptor. *Science* 309, 2222–2226 (2005). [PubMed: 16195464]
21. Bochner DN, Sapp RW, Adelson JD, Zhang S, Lee H, Djuricic M, Syken J, Dan Y, Shatz CJ, Blocking PirB up-regulates spines and functional synapses to unlock visual cortical plasticity and facilitate recovery from amblyopia. *Sci. Transl. Med* 6, 258ra140(2014).
22. Akbik FV, Bhagat SM, Patel PR, Cafferty WBJ, Strittmatter SM, Anatomical plasticity of adult brain is titrated by Nogo Receptor 1. *Neuron* 77, 859–866 (2013). [PubMed: 23473316]
23. McKenzie IA, Ohayon D, Li H, de Faria JP, Emery B, Tohyama K, Richardson WD, Motor skill learning requires active central myelination. *Science* 346, 318–322 (2014). [PubMed: 25324381]
24. Bhagat SM, Butler SS, Taylor JR, McEwen BS, Strittmatter SM, Erasure of fear memories is prevented by Nogo Receptor 1 in adulthood. *Mol. Psychiatry* 21, 1281–1289 (2016). [PubMed: 26619810]
25. Fournier AE, GrandPre T, Strittmatter SM, Identification of a receptor mediating Nogo-66 inhibition of axonal regeneration. *Nature* 409, 341–346 (2001). [PubMed: 11201742]
26. Atwal JK, Pinkston-Gosse J, Syken J, Stawicki S, Wu Y, Shatz C, Tessier-Lavigne M, PirB is a functional receptor for myelin inhibitors of axonal regeneration. *Science* 322, 967–970 (2008). [PubMed: 18988857]
27. Huebner EA, Kim BG, Duffy PJ, Brown RH, Strittmatter SM, A multi-domain fragment of Nogo-A protein is a potent inhibitor of cortical axon regeneration via Nogo receptor 1. *J. Biol. Chem* 286, 18026–18036 (2011). [PubMed: 21454605]
28. Wang X, Chun S-J, Treloar H, Vartanian T, Greer CA, Strittmatter SM, Localization of Nogo-A and Nogo-66 receptor proteins at sites of axon–myelin and synaptic contact. *J. Neurosci* 22, 5505–5515 (2002). [PubMed: 12097502]
29. Venkatesh K, Chivatakarn O, Lee H, Joshi PS, Kantor DB, Newman BA, Mage R, Rader C, Giger RJ, The Nogo-66 receptor homolog NgR2 is a sialic acid-dependent receptor selective for myelin-associated glycoprotein. *J. Neurosci* 25, 808–822 (2005). [PubMed: 15673660]
30. Kim J-E, Liu BP, Park JH, Strittmatter SM, Nogo-66 receptor prevents raphespinal and rubrospinal axon regeneration and limits functional recovery from spinal cord injury. *Neuron* 44, 439–451 (2004). [PubMed: 15504325]
31. Harvey PA, Lee DHS, Qian F, Weinreb PH, Frank E, Blockade of Nogo receptor ligands promotes functional regeneration of sensory axons after dorsal root crush. *J. Neurosci* 29, 6285–6295 (2009). [PubMed: 19439606]
32. Siegel CS, Fink KL, Strittmatter SM, Cafferty WBJ, Plasticity of intact rubral projections mediates spontaneous recovery of function after corticospinal tract injury. *J. Neurosci* 35, 1443–1457 (2015). [PubMed: 25632122]
33. Fink KL, Strittmatter SM, Cafferty WB, Comprehensive corticospinal labeling with *mu-crystallin* transgene reveals axon regeneration after spinal cord trauma in *ngr1*<sup>-/-</sup> mice. *J. Neurosci* 35, 15403–15418 (2015). [PubMed: 26586827]
34. Bonilla IE, Tanabe K, Strittmatter SM, Small proline-rich repeat protein 1A is expressed by axotomized neurons and promotes axonal outgrowth. *J. Neurosci* 22, 1303–1315 (2002). [PubMed: 11850458]
35. Tanabe K, Bonilla I, Winkles JA, Strittmatter SM, Fibroblast growth factor-inducible-14 is induced in axotomized neurons and promotes neurite outgrowth. *J. Neurosci* 23, 9675–9686 (2003). [PubMed: 14573547]



36. Costigan M, Befort K, Karchewski L, Griffin RS, D'Urso D, Allchorne A, Sitariski J, Mannion JW, Pratt RE, Woolf CJ, Replicate high-density rat genome oligonucleotide microarrays reveal hundreds of regulated genes in the dorsal root ganglion after peripheral nerve injury. *BMC Neurosci* 3, 16(2002). [PubMed: 12401135]
37. Seiffers R, Mills CD, Woolf CJ, ATF3 increases the intrinsic growth state of DRG neurons to enhance peripheral nerve regeneration. *J. Neurosci* 27, 7911–7920 (2007). [PubMed: 17652582]
38. Omura T, Omura K, Tedeschi A, Riva P, Painter MW, Rojas L, Martin J, Lisi V, Huebner EA, Latremoliere A, Yin Y, Barrett LB, Singh B, Lee S, Crisman TJ, Gao F, Li S, Kapur K, Geschwind DH, Kosik KS, Coppola G, He Z, Carmichael ST, Benowitz LI, Costigan M, Woolf CJ, Robust axonal regeneration occurs in the injured CAST/Ei Mouse CNS. *Neuron* 86, 1215–1227 (2015). [PubMed: 26004914]
39. Meunier J-C, Mollereau C, Toll L, Suaudeau C, Moisand C, Alvinerie P, Butour J-L, Guillemot J-C, Ferrara P, Monsarrat B, Mazarguil H, Vassart G, Parmentier M, Costentin J, Isolation and structure of the endogenous agonist of opioid receptor-like ORL<sub>1</sub> receptor. *Nature* 377, 532–535 (1995). [PubMed: 7566152]
40. Briscini L, Corradini L, Ongini E, Bertorelli R, Up-regulation of ORL-1 receptors in spinal tissue of allodynic rats after sciatic nerve injury. *Eur. J. Pharmacol* 447, 59–65 (2002). [PubMed: 12106803]
41. Wang KC, Kim JA, Sivasankaran R, Segal R, He Z, p75 interacts with the Nogo receptor as a co-receptor for Nogo, MAG and OMgp. *Nature* 420, 74–78 (2002). [PubMed: 12422217]
42. Robak LA, Venkatesh K, Lee H, Raiker SJ, Duan Y, Lee-Osbourne J, Hofer T, Mage RG, Rader C, Giger RJ, Molecular basis of the interactions of the Nogo-66 receptor and its homolog NgR2 with myelin-associated glycoprotein: Development of NgR<sup>OMNI</sup>-Fc, a novel antagonist of CNS myelin inhibition. *J. Neurosci* 29, 5768–5783 (2009). [PubMed: 19420245]
43. Elhammer A, Kornfeld S, Two enzymes involved in the synthesis of O-linked oligosaccharides are localized on membranes of different densities in mouse lymphoma BW5147 cells. *J. Cell Biol* 99, 327–331 (1984). [PubMed: 6429158]
44. Johnson DC, Spear PG, O-linked oligosaccharides are acquired by herpes simplex virus glycoproteins in the Golgi apparatus. *Cell* 32, 987–997 (1983). [PubMed: 6299584]
45. Piller V, Piller F, Fukuda M, Biosynthesis of truncated O-glycans in the T cell line Jurkat. Localization of O-glycan initiation. *J. Biol. Chem* 265, 9264–9271 (1990). [PubMed: 2140570]
46. Wen D, Wildes CP, Silvan L, Walus L, Mi S, Lee DHS, Meier W, Pepinsky RB, Disulfide structure of the leucine-rich repeat C-terminal cap and C-terminal stalk region of Nogo-66 receptor. *Biochemistry* 44, 16491–16501 (2005). [PubMed: 16342940]
47. McLeod RL, Parra LE, Mutter JC, Erickson CH, Carey GJ, Tulshian DB, Fawzi AB, Smith-Torhan A, Egan RW, Cuss FM, Hey JA, Nociceptin inhibits cough in the guinea-pig by activation of ORL<sub>1</sub> receptors. *Br. J. Pharmacol* 132, 1175–1178 (2001). [PubMed: 11250866]
48. McLeod RL, Tulshian DB, Bolser DC, Varty GB, Baptista M, Fernandez X, Parra LE, Zimmer JC, Erickson CH, Ho GD, Jia Y, Ng FW, Korfmacher W, Xu X, Veals J, Smith-Torhan A, Wainhaus S, Fawzi AB, Austin TM, van Heek M, Hey JA, Pharmacological profile of the NOP agonist and cough suppressing agent SCH 486757 (8-[Bis(2-Chlorophenyl)Methyl]-3-(2-Pyrimidinyl)-8-Azabicyclo[3.2.1]Octan-3-Ol) in preclinical models. *Eur. J. Pharmacol* 630, 112–120 (2010). [PubMed: 20006596]
49. Mittal N, Roberts K, Pal K, Bentolila LA, Fultz E, Minasyan A, Cahill C, Pradhan A, Conner D, DeFea K, Evans C, Walwyn W, Select G-protein-coupled receptors modulate agonist-induced signaling via a ROCK, LIMK, and  $\beta$ -arrestin 1 pathway. *Cell Rep* 5, 1010–1021 (2013). [PubMed: 24239352]
50. Alder J, Kallman S, Palmieri A, Khadim F, Ayer JJ, Kumar S, Tsung K, Grinberg I, Thakker-Varia S, Neuropeptide orphanin FQ inhibits dendritic morphogenesis through activation of RhoA. *Dev. Neurobiol* 73, 769–784 (2013). [PubMed: 23821558]
51. Jin Z, Strittmatter SM, Rac1 mediates collapsin-1-induced growth cone collapse. *J. Neurosci* 17, 6256–6263 (1997). [PubMed: 9236236]
52. Fournier AE, Takizawa BT, Strittmatter SM, Rho kinase inhibition enhances axonal regeneration in the injured CNS. *J. Neurosci* 23, 1416–1423 (2003). [PubMed: 12598630]

53. Duffy P, Schmandke A, Schmandke A, Sigworth J, Narumiya S, Cafferty WBJ, Strittmatter SM, Rho-associated kinase II (ROCKII) limits axonal growth after trauma within the adult mouse spinal cord. *J. Neurosci* 29, 15266–15276 (2009). [PubMed: 19955379]
54. Viaro R, Sanchez-Pernaute R, Marti M, Trapella C, Isacson O, Morari M, Nociceptin/orphanin FQ receptor blockade attenuates MPTP-induced parkinsonism. *Neurobiol. Dis* 30, 430–438 (2008). [PubMed: 18413287]
55. Basso DM, Fisher LC, Anderson AJ, Jakeman LB, McTigue DM, Popovich PG, Basso Mouse Scale for locomotion detects differences in recovery after spinal cord injury in five common mouse strains. *J. Neurotrauma* 23, 635–659 (2006). [PubMed: 16689667]
56. Fink KL, López-Giráldez F, Kim I-J, Strittmatter SM, Cafferty WBJ, Identification of intrinsic axon growth modulators for intact CNS neurons after Injury. *Cell Rep* 18, 2687–2701 (2017). [PubMed: 28297672]
57. McDonald J, Barnes TA, Okawa H, Williams J, Calo G, D. J. Rowbotham, D. G. Lambert, Partial agonist behaviour depends upon the level of nociceptin/orphanin FQ receptor expression: Studies using the ecdysone-inducible mammalian expression system. *Br. J. Pharmacol* 140, 61–70 (2003). [PubMed: 12967935]
58. Hawes BE, Graziano MP, Lambert DG, Cellular actions of nociceptin: Transduction mechanisms. *Peptides* 21, 961–967 (2000). [PubMed: 10998529]
59. Cai D, Shen Y, De Bellard M, Tang S, Filbin MT, Prior exposure to neurotrophins blocks inhibition of axonal regeneration by MAG and myelin via a cAMP-dependent mechanism. *Neuron* 22, 89–101 (1999). [PubMed: 10027292]
60. Cafferty WBJ, Duffy P, Huebner E, Strittmatter SM, MAG and OMgp synergize with Nogo-A to restrict axonal growth and neurological recovery after spinal cord trauma. *J. Neurosci* 30, 6825–6837 (2010). [PubMed: 20484625]
61. Budel S, Padukkavidana T, Liu BP, Feng Z, Hu F, Johnson S, Lauren J, Park JH, McGee AW, Liao J, Stillman A, Kim J-E, Yang B-Z, Sodi S, Gelernter J, Zhao H, Hisama F, Arnsten AFT, Strittmatter SM, Genetic variants of Nogo-66 receptor with possible association to schizophrenia block myelin inhibition of axon growth. *J. Neurosci* 28, 13161–13172 (2008). [PubMed: 19052207]
62. Nakamura F, Tanaka M, Takahashi T, Kalb RG, Strittmatter SM, Neuropilin-1 extracellular domains mediate semaphorin D/III-induced growth cone collapse. *Neuron* 21, 1093–1100 (1998). [PubMed: 9856464]
63. Laurén J, Hu F, Chin J, Liao J, Airaksinen MS, Strittmatter SM, Characterization of myelin ligand complexes with neuronal Nogo-66 receptor family members. *J. Biol. Chem* 282, 5715–5725 (2007). [PubMed: 17189258]
64. Beedle AM, McRory JE, Poirot O, Doering CJ, Altier C, Barrere C, Hamid J, Nargeot J, Bourinet E, Zamponi GW, Agonist-independent modulation of N-type calcium channels by ORL1 receptors. *Nat. Neurosci* 7, 118–125 (2004). [PubMed: 14730309]
65. Zou Y, Stagi M, Wang X, Yigitkanli K, Siegel CS, Nakatsu F, Cafferty WBJ, Strittmatter SM, Gene-silencing screen for mammalian axon regeneration identifies *Inpp5f* (*Sac2*) as an endogenous suppressor of repair after spinal cord injury. *J. Neurosci* 35, 10429–10439 (2015). [PubMed: 26203138]
66. Starkey ML, Barritt AW, Yip PK, Davies M, Hamers FPT, McMahon SB, Bradbury EJ, Assessing behavioural function following a pyramidotomy lesion of the corticospinal tract in adult mice. *Exp. Neurol* 195, 524–539 (2005). [PubMed: 16051217]

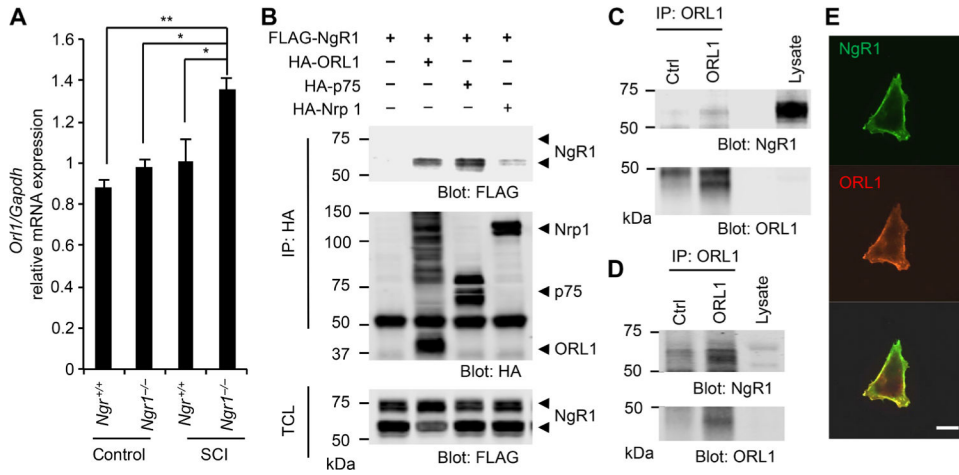


**Fig. 1. NgR1 interacts with ORL1.**

(A) The levels of the *ORL1* mRNA normalized to those of a *Gapdh* internal control in the brain stem. Tissues were collected from *Ngr1*<sup>+/+</sup> or *Ngr1*<sup>-/-</sup> mice 4 days after sham operation or spinal cord injury (SCI) ( $n = 3$  mice for each group). Data are means  $\pm$  SE. \* $P < 0.05$ , \*\* $P < 0.001$ , one-way analysis of variance (ANOVA) followed by Tukey's test. (B) Human embryonic kidney–293T (HEK293T) cells were transfected with FLAG-NgR1 alone or with hemagglutinin (HA)–ORL1, HA-p75, or HA-neuropilin. HA immunoprecipitates were immunoblotted for HA and FLAG. Means  $\pm$  SE,  $n = 3$  independent experiments. TCL, total cell lysates. (C and D) ORL1 immunoprecipitates from mouse forebrain (E) or hippocampal neurons at 21 DIV (days in vitro) (G) were immunoblotted for NgR1 and ORL1.  $n = 3$  independent experiments. Ctrl, control. (E) Cos7 cells transfected with FLAG-NgR1 and HA-ORL1 were stained for FLAG and HA without permeabilization. Means  $\pm$  SE,  $n = 3$  independent experiments. Scale bar, 20  $\mu$ m.

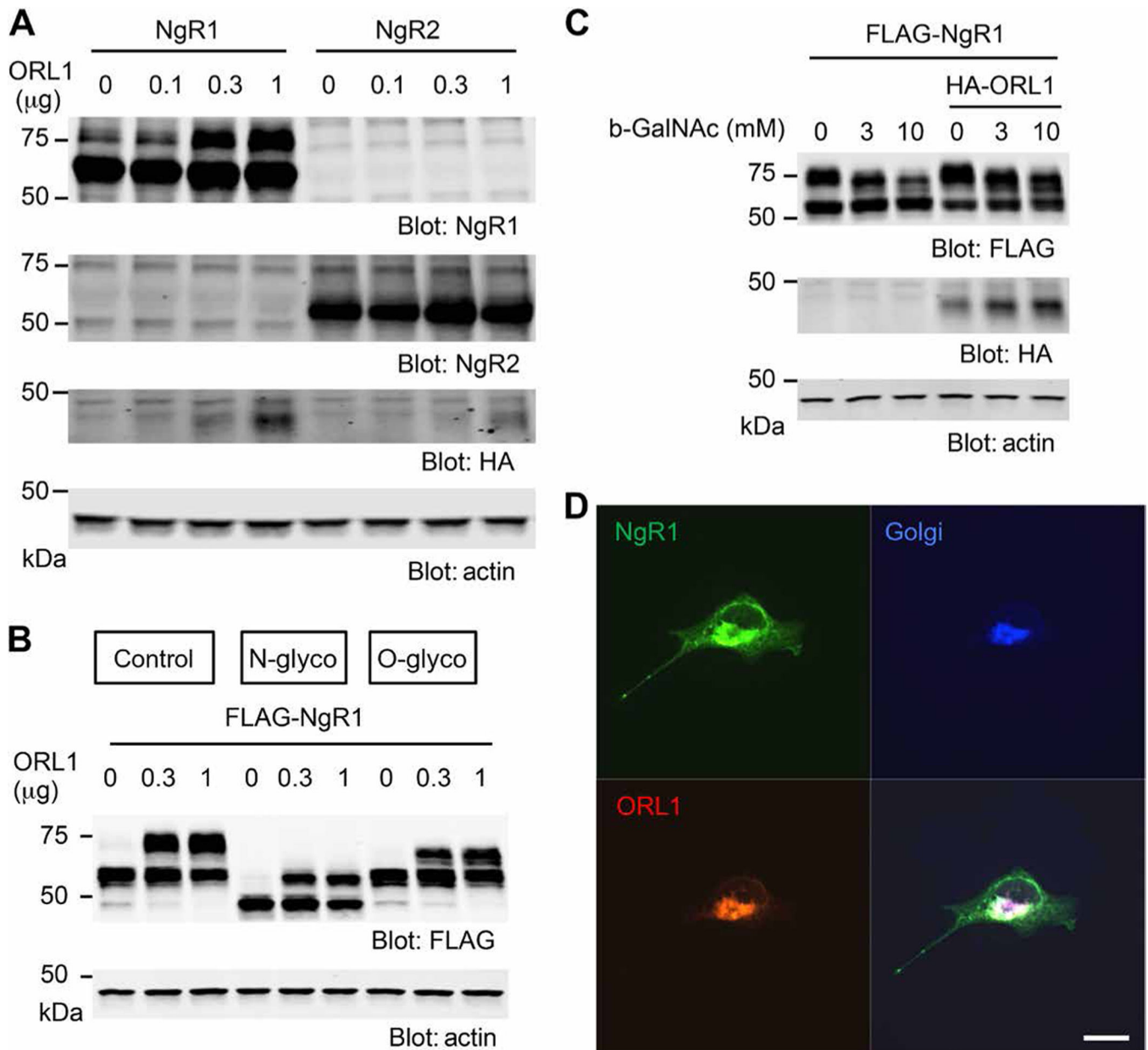


**Fig. 2. ORL1 enhances O-linked glycosylation of NgR1 at Golgi body.** (A) HEK293T cells were transfected with Myc-NgR1 or Myc-NgR2, with or without HA-ORL1. HA immunoprecipitates were immunoblotted for HA and Myc. Means  $\pm$  SE,  $n = 3$  independent experiments. (B) HEK293T cells were transfected with FLAG-NgR1 and increasing amounts of HA-ORL1 and treated without or with N-glycosidase or O-glycosidase for 1 hour. Cell lysates were immuno-blotted for FLAG or actin. Means  $\pm$  SE,  $n = 3$  independent experiments. glyco, glycosidase. (C) HEK293T cells were transfected with FLAG-NgR1, with or without HA-ORL1 and treated with dimethyl sulfoxide or increasing amounts of benzyl-*N*-acetyl- $\alpha$ -D-galactosaminide (b-GalNAc) as indicated. Cell lysates were immunoblotted for FLAG, HA, and actin. Means  $\pm$  SE,  $n = 4$  independent experiments.

**(D)** Cos7 cells cotransfected with FLAG-NgR1 and HA-ORL1 were stained with NgR1, HA, and GM130 antibodies. Means  $\pm$  SE,  $n = 3$  independent experiments. Scale bar, 20  $\mu$ m.

Author Manuscript

Author Manuscript

Author Manuscript

Author Manuscript

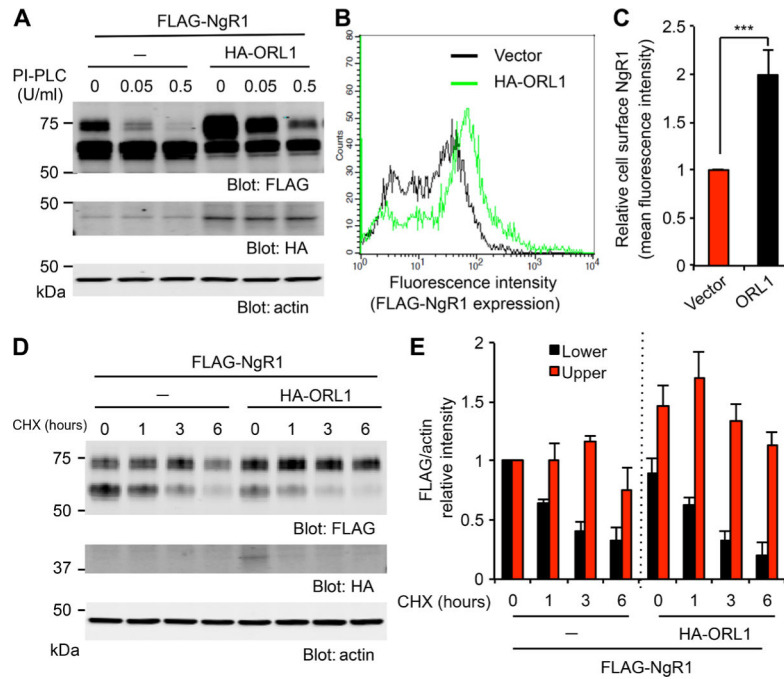


**Fig. 3. ORL1 increases the cell surface expression of NgR1.**

(A) HEK293T cells were transfected with FLAG-NgR1, with or without HA-ORL1, and treated with phosphatidylinositol-specific phospholipase C (PI-PLC) at the indicated amounts for 1 hour. Cell lysates were immunoblotted for FLAG, HA, and actin. Means  $\pm$  SE,  $n = 3$  independent experiments. (B and C) Cos7 cells stably expressing FLAG-NgR1 were transfected with control vector or HA-ORL1 and stained for FLAG. Cells were analyzed by flow cytometry (B). The graph shows the mean fluorescence intensity from three independent experiments with  $\pm$ SE (C). \*\*\* $P < 0.005$ , Student's two-tailed  $t$  test. (D) HEK293T cells were transfected with FLAG-NgR1 with or without HA-ORL1 and treated with cycloheximide (CHX; 10  $\mu$ g/ml) for the indicated periods. Cell lysates were immunoblotted for FLAG, HA, and actin. (E) Quantification of NgR1 upper or lower bands normalized to actin of control or ORL1-transfected cells. Means  $\pm$  SE,  $n = 4$  independent experiments.

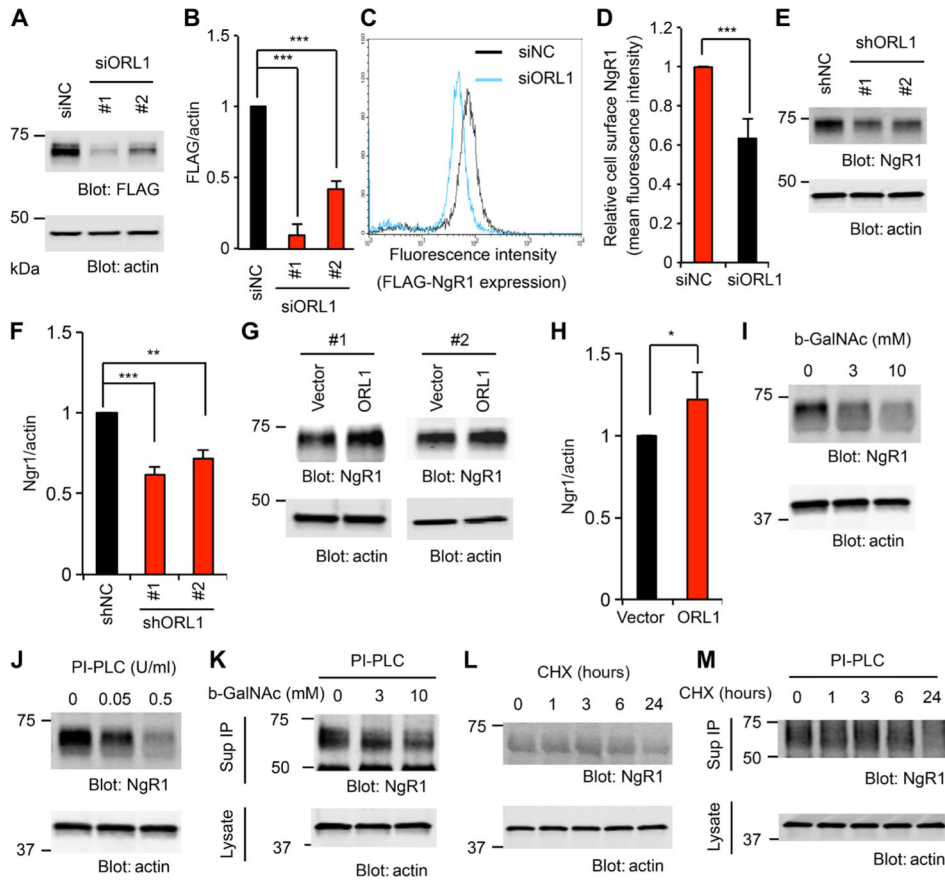


**Fig. 4. Reduction of ORL1 decreases Ngr1 expression in Neuro2A and neurons.** (A and B) Neuro2A cells stably expressing FLAG-Ngr1 were transfected with control, ORL1 #1, or ORL1 #2 small interfering RNA (siRNA). Cell lysates were immunoblotted for FLAG and actin (A). Quantification of FLAG-Ngr1 protein levels in the lysates normalized to actin from three independent experiments (B). Means  $\pm$  SE. \*\*\* $P$  < 0.005, one-way ANOVA followed by Tukey's test. (C and D) Neuro2A cells stably expressing FLAG-Ngr1 were transfected with control or ORL1 siRNA. After 36 hours, cells were fixed, stained for FLAG, and analyzed by flow cytometry (C). The graph shows the mean fluorescence intensity from three independent experiments  $\pm$  SE (D). \*\*\* $P$  < 0.005, Student's two-tailed  $t$  test. siNC, nontargeting control small interfering RNA. (E and F) Cortical neurons were transduced with lentiviral vector for control, ORL1 short hairpin RNA (shRNA) #1, or ORL1 shRNA #2 at 3 DIV. Cell lysates were immunoblotted for Ngr1 and actin (E). The graph shows the quantification of Ngr1 protein levels in the lysates normalized to actin from four independent experiments (F). Means  $\pm$  SE. \*\*\* $P$  < 0.005, \*\* $P$  < 0.01, one-way ANOVA followed by Tukey's test. (G and H) Cortical neurons were nucleofected with control vector or HA-ORL1. Cell lysates were immunoblotted for Ngr1 and actin (G). The graph shows the quantification of Ngr1 protein levels in the lysates normalized to actin from three independent experiments (H). Means  $\pm$  SE. \* $P$  < 0.05, Student's two-tailed  $t$  test. (I and J) Cortical neurons at 10 DIV were treated with the indicated concentrations of b-GalNAc for 24 hours (I) and PI-PLC for 1 hour (J). Cell lysates were immuno-blotted for Ngr1 and actin.  $n$  = 4 independent experiments. (K) Cortical neurons at 10 DIV were

treated with indicated concentrations of b-GalNAc for 24 hours, and culture medium was replaced with PI-PLC-containing medium for 1 hour. NgR1 immunoprecipitates from the culture medium and cell lysates were immunoblotted for NgR1 and actin, respectively.  $n = 3$  independent experiments. **(L)** Cortical neurons at 10 DIV were treated with CHX (10  $\mu\text{g}/\text{ml}$ ) for indicated times. Cell lysates were immunoblotted for NgR1 and actin.  $n = 4$  independent experiments. **(M)** Cortical neurons at 10 DIV were treated with CHX (10  $\mu\text{g}/\text{ml}$ ) for an indicated time, and culture medium was replaced with PI-PLC-containing medium for 1 hour. NgR1 immunoprecipitates from the culture medium and cell lysates were immunoblotted for NgR1 and actin, respectively.  $n = 4$  independent experiments.



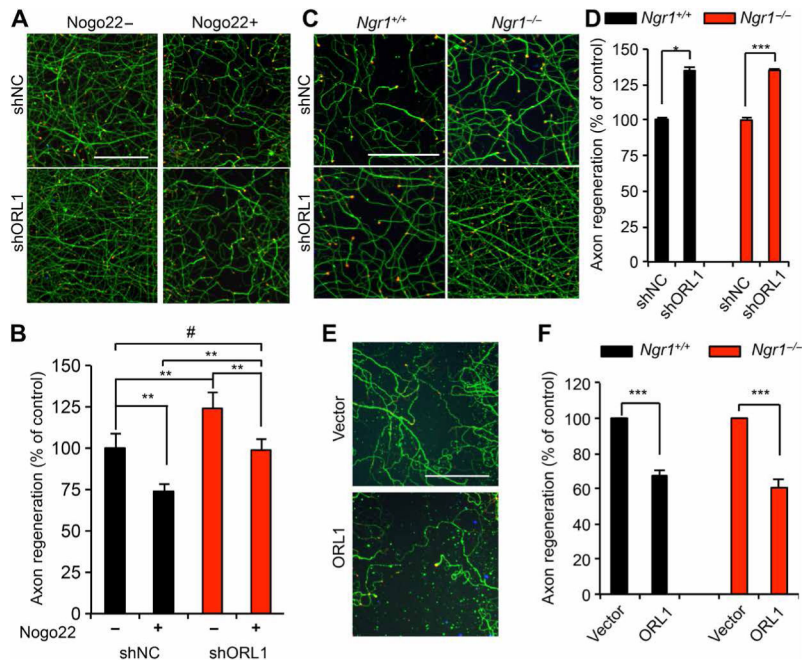


**Fig. 5. ORL1 inhibits axon regeneration.**

(A and B) Cortical neurons were transduced with lentiviral vector for control or ORL1 shRNA at 3 DIV. Axons were scraped at 8 DIV and allowed to regenerate for 3 days in the presence of vehicle or Nogo22 (100 nM). The microphotographs show  $\beta$ III-tubulin (in axons; green) and phalloidin (to stain F-actin; red) to illustrate the growth cones of cortical neurons in the middle of the scraped area (A). Scale bar, 100  $\mu$ m. The graph shows quantification of axon regeneration (B). Means  $\pm$  SE.  $n = 10$  biological replicates,  $**P < 0.01$ , #not significant, one-way ANOVA followed by Tukey's test. (C and D) Cortical neurons were transduced with lentiviral vector for control or ORL1 shRNA at 3 DIV. Axons were scraped at 8 DIV and allowed to regenerate for 3 days. Images are of the scraped areas from *Ngr1*<sup>+/+</sup> and *Ngr1*<sup>-/-</sup> cultures (C). Scale bar, 100  $\mu$ m. The graph shows quantification of axon regeneration (D). Means  $\pm$  SE.  $n = 4$  biological replicates,  $***P < 0.005$ ,  $*P < 0.05$ , Student's two-tailed  $t$  test. (E and F) Cortical neurons were nucleofected with control vector or HA-ORL1. Axons were scraped at 8 DIV and allowed to regenerate for 3 days. Images are of the scraped area from *Ngr1*<sup>+/+</sup> cultures (E). Scale bar, 100  $\mu$ m. The graph shows quantification of axon regeneration (F). Data are means  $\pm$  SE.  $n = 3$  biological replicates,  $***P < 0.005$ , Student's two-tailed  $t$  test.

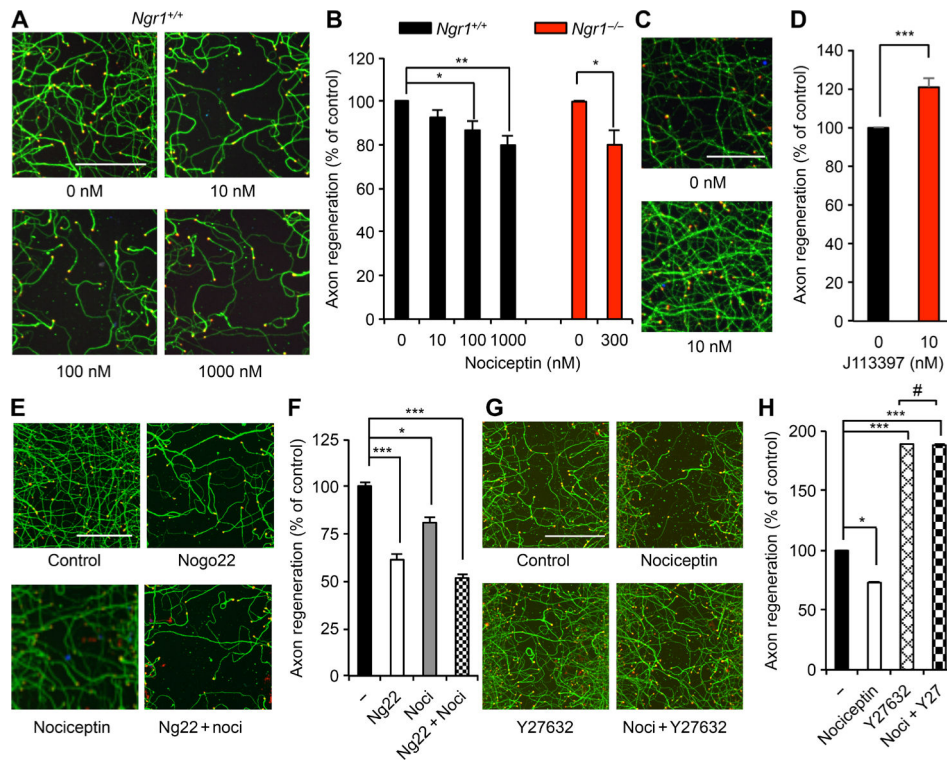


**Fig. 6. Nociceptin inhibits axonal regeneration in the absence of NgR1.**

(A and B) Cortical neurons were scraped and treated with an indicated amount of nociceptin at 8 DIV for 3 days (A). Scale bar, 100 μm. The graph shows quantification of axonal regeneration (B). Means ± SE. *n* = 4 biological replicates, \**P* < 0.05, \*\**P* < 0.01, one-way ANOVA followed by Dunnett's test (*Ngr1*<sup>+/+</sup>), Student's two-tailed *t* test (*Ngr1*<sup>-/-</sup>). (C and D) Cortical neurons were scraped and treated with J113397 at 8 DIV for 3 days (C). Scale bar, 100 μm. The graph shows quantification of axon regeneration (D). Means ± SE. *n* = 4 biological replicates, \*\*\**P* < 0.005, Student's two-tailed *t* test. (E and F) Cortical neurons were scraped and treated with vehicle, Nogo22 (100 nM), nociceptin (300 nM), or Nogo22 (100 nM) + nociceptin (noci; 300 nM) at 8 DIV for 3 days (E). Scale bar, 100 μm. The graph shows quantification of axonal regeneration (F). Means ± SE. *n* = 5 biological replicates, \*\*\**P* < 0.005, \**P* < 0.05, one-way ANOVA followed by Tukey's test. (G and H) Cortical neurons were scraped and treated with vehicle, nociceptin (300 nM), or nociceptin (300 nM) + Y27632 (100 nM) at 8 DIV for 3 days (G). Scale bar, 100 μm. The graph shows quantification of axonal regeneration (H). Means ± SE. *n* = 5 biological replicates, \**P* < 0.05, \*\*\**P* < 0.005, #not significant, one-way ANOVA followed by Tukey's test.

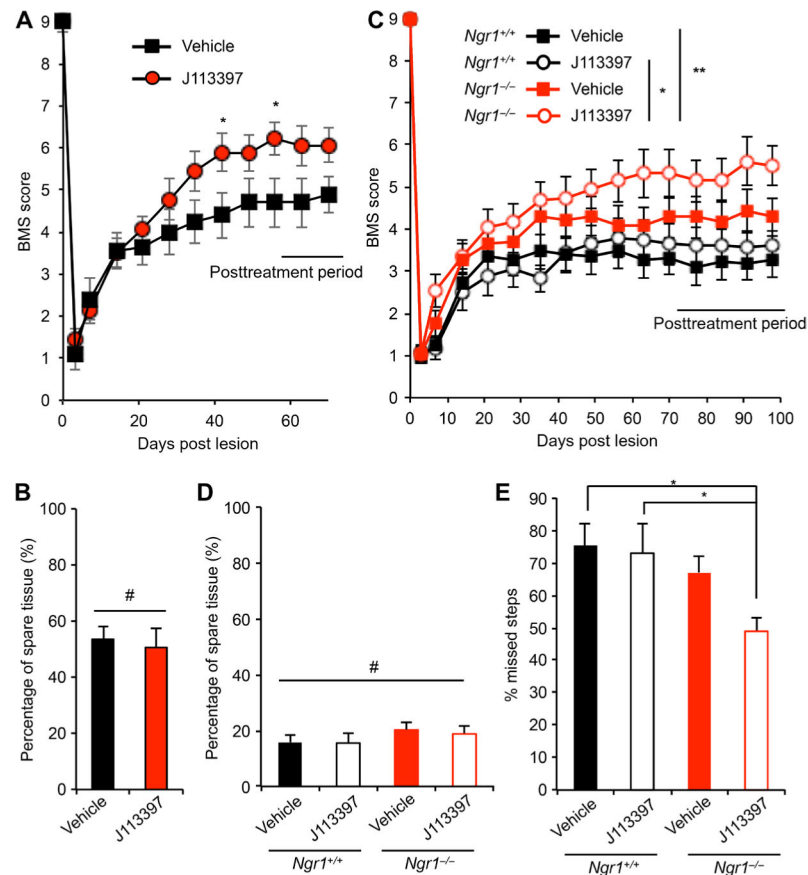


**Fig. 7. Administration of the ORL1 antagonist J113397 improves recovery from SCI.** (A) Open-field locomotion performance as assessed by the BMS of vehicle- and J113397-injected WT mice. Animals were scored on days 0, 3, 7, 14, 21, 28, 35, 42, 49, 56, 63, and 70 by two experienced observers who were blinded to the group. Means  $\pm$  SE.  $n = 10$  vehicle-injected mice and  $n = 9$  J113397-injected mice.  $*P = 0.022$ , repeated-measures ANOVA for treatment effect across last five time points. (B) The extent of spared tissue at the injury site was quantified. Data are presented as means  $\pm$  SE.  $n = 10$  vehicle-injected mice and  $n = 9$  J113397-injected mice. No significant differences between groups. Student's two-tailed  $t$  test. (C) Open-field locomotion performance as assessed by the BMS of WT and *Ngr1*<sup>-/-</sup> mice after T7 dorsal overhemisection and treatment with vehicle or J113397. Animals were scored on days 0, 3, 7, 14, 21, 28, 35, 42, 49, 56, 63, 70, 77, 84, 91, and 98 by two experienced observers who were blinded to the group. Means  $\pm$  SE.  $n = 14$  mice in each group.  $*P = 0.010$ , repeated-measures ANOVA for group effect across last six time points, and  $*P < 0.05$ ,  $**P < 0.01$ , significant difference between indicated pairs by repeated-measures ANOVA with Tukey's multiple comparison test. (D) The extent of spared tissue at the injury site was quantified. Means  $\pm$  SE.  $n = 14$  mice in each group. No significant differences between groups. One-way ANOVA. (E) Gridwalk test at day 80 after injury. Means  $\pm$  SE.  $n = 14$  mice in each group.  $*P < 0.05$ , one-way ANOVA followed by Tukey's test.

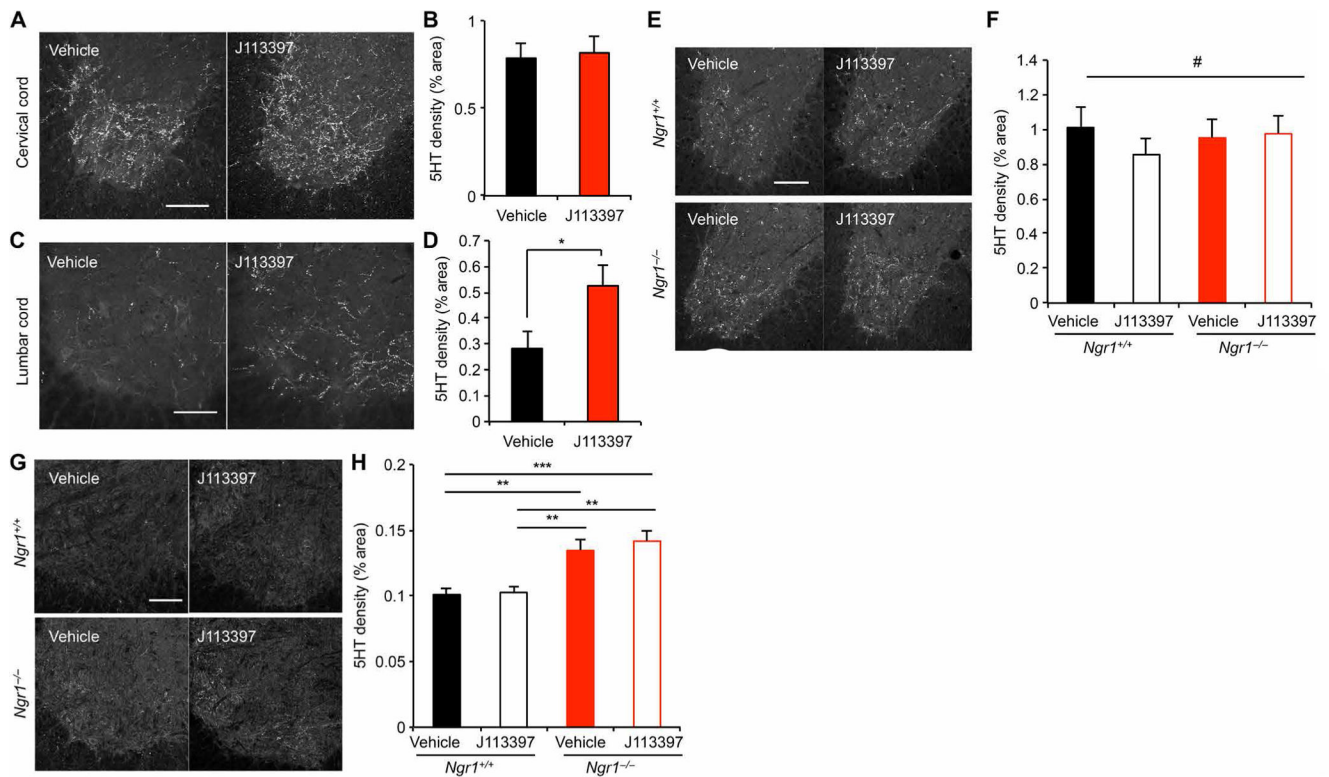


**Fig. 8. Administration of the ORL1 antagonist J113397 increases raphespinal axon growth after SCI.**

(A and C) Raphespinal axon sprouting in WT animals. Representative image of raphespinal fibers stained for 5HT in the spinal ventral horn. Coronal sections of cervical (A) and lumbar (C) were from vehicle- and J113397-treated mice at 72 days after hemisection. Scale bar, 100  $\mu$ m. (B and D) Quantification of 5HT+ fiber density in WT animals. Means  $\pm$  SE.  $n = 7$  vehicle- injected mice and  $n = 7$  J113397-injected mice. #No significant difference (B),  $*P < 0.05$  (D), Student's two-tailed  $t$  test. (E and G) Representative image of raphespinal fibers stained for 5HT in the spinal ventral horn. Coronal sections of cervical (E) and lumbar (G) were from vehicle- and J113397-treated mice from each genotype at 98 days after overhemisection. Scale bar, 100  $\mu$ m. (F and H) Quantification of 5HT+ fiber density. Means  $\pm$  SE.  $n = 14$  mice for each group, #no significant differences (F),  $**P < 0.01$ ,  $***P < 0.005$  (H), one-way ANOVA followed by Tukey's test.